# Reduced Sea Ice Enhances Intensification of Winter Storms over the Arctic Ocean

ALEX D. CRAWFORD,[a] JENNIFER V. LUKOVICH,[a] MICHELLE R. MCCRYSTALL,[a] JULIENNE C. STROEVE,[a,b,c] AND DAVID G. BARBER[a]

[a] *Centre for Earth Observation Science, University of Manitoba, Winnipeg, Manitoba, Canada*
[b] *Department of Earth Sciences, University College London, London, United Kingdom*
[c] *National Snow and Ice Data Center, Cooperative Institute for Research in Environmental Science, University of Colorado Boulder, Boulder, Colorado*

(Manuscript received 24 September 2021, in final form 26 January 2022)

ABSTRACT: The ideal environment for extratropical cyclone development includes strong vertical shear of horizontal wind and low static stability in the atmosphere. Arctic sea ice loss enhances the upward flux of energy to the lower atmosphere, reducing static stability. This suggests that Arctic sea ice loss may facilitate more intense storms over the Arctic Ocean. However, prior research into this possibility has yielded mixed results with uncertain cause and effect. This work has been limited either in scope (focusing on a few case studies) or resolution (focusing on seasonal averages). In this study, we extend this body of research by comparing the intensification rate and maximum intensity of individual cyclones to local sea ice anomalies. We find robust evidence that reduced sea ice in winter (December–March) strengthens Arctic cyclones by enhancing the surface turbulent heat fluxes and lessening static stability while also strengthening vertical shear of horizontal wind. We find weaker evidence for this connection in spring (April–June). In both seasons, lower sea ice concentration also enhances cyclone-associated precipitation. Although reduced sea ice also weakens static stability in September/October (when sea ice loss has been especially acute), this does not translate to stronger storms because of coincident weakening of wind shear. Sea ice anomalies also have little or no connection to cyclone-associated precipitation in these months. Therefore, future sea ice reductions (e.g., related to delayed autumn freeze-up) will likely enhance Arctic cyclone intensification in winter and spring, but this relationship is sensitive to simultaneous connections between sea ice and wind shear.

SIGNIFICANCE STATEMENT: Sea ice is a barrier between the ocean and atmosphere, limiting the exchange of energy between them. As the amount of sea ice in the Arctic Ocean declines, the ocean can transfer more heat to the atmosphere above in fall and winter. It is theorized that this extra energy may help intensify storms that pass through the Arctic. We examine individual storms over the Arctic Ocean and what sea ice conditions they experience as they develop. We find that storms intensify more when sea ice is lower than normal in the winter season only. This relationship may contribute to stronger Arctic winter storms in the future, including heavier precipitation and stronger winds (which can enhance wave heights and coastal erosion).

KEYWORDS: Arctic; Sea ice; Extratropical cyclones; Atmosphere-ocean interaction

## 1. Introduction

Severe reduction in Arctic sea ice volume and extent in recent decades has been a conspicuous manifestation of modern climate change (Stroeve et al. 2012; IPCC 2013; Kwok 2018). Although most prominent in September, Arctic sea ice decline is observable in all months and across all Arctic subregions (Onarheim et al. 2018; Stroeve and Notz 2018; Serreze and Meier 2019). Removal of the sea ice cover permits greater sensible and latent heat fluxes from ocean to atmosphere in autumn/winter (Royer et al. 1990; Deser et al. 2000; Serreze et al. 2009; Screen et al. 2013). Indeed, even small reductions in sea ice concentration (SIC), such as the opening of a lead, can generate sensible heat fluxes exceeding 50 W $m^2$ (Walter et al. 1995; Raddatz et al. 2012). Additionally, the autumn/winter sensible heat flux may be enhanced by additional heat uptake by open water compared to sea ice surfaces during summer (Serreze et al. 2009; Screen and Simmonds 2010; Kashiwase et al. 2017).

Reduced sea ice and amplified warming may in turn impact local development of synoptic-scale cyclones (hereafter simply "cyclones" or "storms"). Such storms can present compound hazards for Arctic communities (e.g., high winds and heavy precipitation). Atmospheric heating by enhanced energy fluxes from anomalously open water is greatest near the surface (Rinke et al. 2006; Serreze et al. 2009; Screen and Simmonds 2010), which reduces static stability (Schweiger et al. 2008; Bader et al. 2011; Jaiser et al. 2012; Koyama et al. 2017). Any reduction in static stability yields more favorable

Denotes content that is immediately available upon publication as open access.

Supplemental information related to this paper is available at the Journals Online website: https://doi.org/10.1175/JCLI-D-21-0747.s1.

*Corresponding author*: Alex D. Crawford, alex.crawford@umanitoba.ca

DOI: 10.1175/JCLI-D-21-0747.1

conditions for cyclone development, which may encourage more frequent or intense storms (Ledrew 1984; Bader et al. 2011; Jaiser et al. 2012). Reductions in surface roughness and static stability that correspond with sea ice loss are also associated with enhanced 10-m winds in climate model simulations (Seo and Yang 2013; Mioduszewski et al. 2018).

Studies examining potential correlations between sea ice loss and Arctic cyclone development have yielded mixed results. In three case studies of Arctic Ocean cyclones from June to September 1976, Ledrew (1984) found that surface enthalpy fluxes were directed downward, counteracting storm development regardless of sea ice conditions. However, an upward surface enthalpy flux contributed to intensification of a mid-October storm that passed over the refreezing sea ice pack. Simmonds and Keay (2009) found significant correlations between 1979 and 2008 September Arctic sea ice extent and both latent heat fluxes and storm intensity over the Arctic Ocean, but no significant correlation with storm frequency. Koyama et al. (2017) found no widespread or consistent differences in the frequency or intensity of autumn (September–November; 1979–2014) storms over the Arctic Ocean and September sea ice extent. By contrast, Valkonen et al. (2021) found that both cyclone frequency and intensity were higher during the cold season (December–May; 1979–2015) when cold-season SIC was lower. However, they found no connection between warm-season (June–November) SIC and warm-season cyclones or cyclones in the subsequent cold season. Each of these seasonal studies used different periods of analysis, seasonal definitions, and atmospheric reanalyses, which may account for some of the differences. Overall, a link between sea ice and storm intensity is better supported than a link with storm frequency.

Baroclinic instability, and therefore the development of synoptic-scale cyclones, depends not only on static stability but also on horizontal temperature gradients (Eady 1949; Pierrehumbert and Swanson 1995; Simmonds and Li 2021), which sea ice conditions can also modify. For example, a distinct temperature gradient between warm open water and the sea ice pack commonly occurs in the East Greenland Sea, which makes the area favorable for storm development. Therefore, shifts in the sea ice edge can cause cyclone development to shift location, too (Deser et al. 2000). Sea ice loss may also have remote influences on extratropical cyclone activity via changes to large-scale circulation (Murray and Simmonds 1995; Alexander et al. 2004; Seierstad and Bader 2008; Crasemann et al. 2017; Wei et al. 2017).

Complicating any examination of how sea ice loss impacts storm development, synoptic-scale storms can also influence the sea ice cover. In winter, synoptic-scale cyclones account for much of the snowfall on sea ice, especially in the Atlantic sector (Webster et al. 2019). They also transport warm, moist air from more southerly latitudes, enhancing downwelling longwave radiation, which inhibits radiative heat loss and sea ice growth (Graham et al. 2019a). During summer storm events, increased cloudiness reduces downwelling shortwave radiation, which inhibits sea ice loss (Wernli and Papritz 2018; Schreiber and Serreze 2020). Strong winds associated with some cyclones can also break up and redistribute sea ice floes (divergence), cause ridging and thickening (convergence), or stir up warmer water masses that often underlie the Arctic's surface mixed layer (Yang et al. 2004; Zhang et al. 2013). Therefore, although cyclones typically depress summer Arctic sea ice loss (Screen et al. 2011; Wernli and Papritz 2018), extreme cyclones can accelerate loss (Zhang et al. 2013; Lukovich et al. 2021).

Recent studies also suggest that sea ice loss enhances cyclone-associated precipitation (CAP). Stroeve et al. (2011) observed greater autumn CAP and total column water vapor in the Atlantic sector of the Arctic Ocean in years with low sea ice extent compared to years with high sea ice extent. Modeling studies show this increase in CAP mostly results from an increase in water vapor available to cyclones rather than a change in cyclone intensity or frequency (Finnis et al. 2007; Li et al. 2014; Crawford and Serreze 2017; Yettella and Kay 2017). However, cause and effect is uncertain since increased precipitation over the Arctic may result from remote enhancement of the latent heat flux followed by increased moisture convergence as well as from local increases to the latent heat flux following sea ice loss (Stroeve et al. 2011; Villamil-Otero et al. 2017).

Most studies of sea ice–cyclone activity linkages described above are either case studies of individual events or large-scale studies examining seasonal sea ice and storm characteristics. The former have limited generalizability, especially to weak or average-strength cyclones. The latter are generalizable but obscure shorter time scales that may better distinguish cause and effect for sea ice–cyclone relations. In this study, we examine thousands of individual Arctic Ocean cyclones, relating daily sea ice conditions to their intensification and associated precipitation. By lagging the sea ice conditions and storm characteristics, we are better able to assess cause and effect. Following past work (Crawford and Serreze 2016; Valkonen et al. 2021), our study area is the central Arctic Ocean and the Beaufort, Chukchi, East Siberian, and Laptev Seas (Fig. 1), roughly corresponding to the climatological (1981–2010) September sea ice extent. Our overarching research questions are the following:

1) Does SIC variability influence the intensification of individual cyclones over the Arctic Ocean?
2) What factors explain seasonal variability in the presence or strength of this relationship?

## 2. Data and methods

### a. *Atmospheric reanalyses*

The latest version of the ECMWF reanalysis (ERA5) uses a hybrid incremental 4D-Var assimilation scheme, incorporates more observational datasets than its predecessor, and includes a weakly coupled land data assimilation system (Hersbach et al. 2020). Hourly surface sensible and latent heat fluxes, total column water, large-scale precipitation, and total precipitation were downloaded for 1979–2019. Instantaneous sea level pressure fields were downloaded with a 3-h interval, as were temperature, horizontal wind, and geopotential height at 1000,

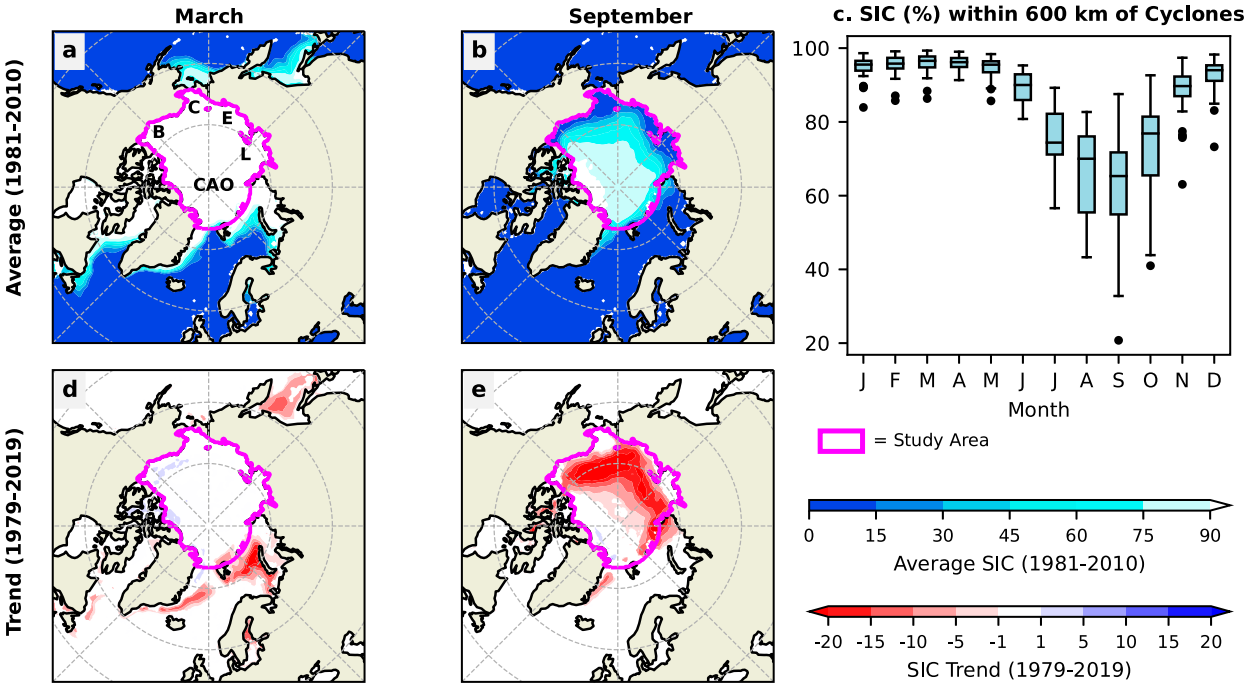


FIG. 1. (a),(b) Average sea ice concentration (SIC; 1981–2010) and (d),(e) its long-term trend (1979–2019) for (a),(d) March and (b),(e) September from the NASA Team algorithm. (c) Monthly average of sea ice concentration within 600 km of cyclone centers passing through the study region (pink line in maps) for the entire study period (1979–2019). Study area comprises the central Arctic Ocean (CAO) and the Beaufort (B), Chukchi (C), East Siberian (E), and Laptev (L) Seas. Boxes in (c) span the interquartile range, with the horizontal line indicating the median, the whiskers extending to the most extreme values within 1.5 times the interquartile range, and dots indicating outliers beyond 1.5 times the interquartile range.

850, and 700 hPa. All fields are available at a 0.25° × 0.25° spatial resolution.

The Modern-Era Retrospective Analysis for Research and Applications version 2 (MERRA-2) uses version 5.12.4 of the Goddard Earth Observing System (GEOS) model and a 3D-Var analysis scheme (Gelaro et al. 2017). Improvements on version 1 of MERRA include better representation of the water cycle, stratospheric ozone, and cryosphere processes and the assimilation of aerosol data. Non-anvil large-scale precipitation, total precipitation, and surface sensible and latent heat fluxes were downloaded as averaged hourly analyzed fields. Sea level pressure and total precipitable water vapor were downloaded as instantaneous 3-h assimilated fields. Temperature, horizontal wind, and geopotential height at 925, 850, and 700 hPa were downloaded as 6-h instantaneous analyzed fields. All fields are available at a 0.5° × 0.625° spatial resolution for the period 1980–2019.

Both reanalyses compared well to temperature, specific humidity, and wind speed measurements from radiosondes launched at about 79°N in Fram Strait in August and September 2017 (Graham et al. 2019c). ERA5 had the highest correlation coefficients and lowest bias and root-mean-square errors. Both products struggled to represent surface inversions during cold stable periods, leading to positive biases in 2-m temperature in winter over sea ice (Graham et al. 2019b) despite correlation coefficients exceeding 0.90 for temperature, surface pressure, and total column water vapor on that same campaign. Correlations with the sensible heat flux in winter were poor for this campaign (0.32 and 0.23 for ERA5 and MERRA-2, respectively). In a comparison to ship- and aircraft-based observations in the Greenland Sea, ERA5 performed better over open water than over the marginal ice zone (Renfrew et al. 2021); however, the standard deviation of observations exceeded the root-mean-square error over both surface conditions for 2-m temperature, 10-m wind, and surface sensible and latent heat fluxes. Additionally, correlation coefficients between ERA5 and ship-based observations exceeded 0.90 for all four variables, showing a realistic contrast for open water versus marginal ice zone environments (Renfrew et al. 2021).

### b. *Sea ice concentration*

The primary sea ice concentration (SIC) datasets used here are taken directly from each reanalysis portal. ERA5 SIC is derived from the Ocean and Sea Ice Satellite Application Facility product [OSI SAF; Table 7 in Hersbach et al. (2020)]. MERRA-2 SIC is derived from several satellite products [Table 3 in Gelaro et al. (2017)]. Although these fields are available at 3-h resolution, both are based in part on the passive microwave satellite retrievals that have a daily (or 2-day) resolution.

Following Valkonen et al. (2021), the NASA Team algorithm is used as an additional source of SIC. This algorithm is applied to passive microwave data from the Scanning Multichannel

Microwave Radiometer (SMMR) aboard *Nimbus-7* and the Special Sensor Microwave/Imagers (SSM/I) and Special Sensor Microwave Imager/Sounder (SSMIS) (Cavalieri et al. 1996). The passive microwave record is bidaily from October 1978 through June 1987 and daily thereafter. Spatial resolution is 25 km × 25 km on a polar stereographic projection. Spatial coverage has a gap centered on the pole with a radius of 611 km through June 1987, 311 km from July 1987 through December 2007, and 94 km thereafter. Data gaps of a single day are filled using bilinear interpolation from adjacent days. December 1987 and January 1988 are omitted from analysis because of a multiweek data gap (3 December 1987 through 12 January 1988). The pole hole is filled by averaging the SIC for all grid cells within 1° latitude of the hole.

The interannual correlation between these datasets for monthly regional SIC in the study area exceeds 0.90 for every month during May–November (when the trend in SIC is strongest), with correlations as low as 0.40 in December–March (Fig. S1 in the online supplemental material). SIC used in MERRA-2 is biased low compared that for ERA5 and the NASA Team algorithm (Fig. S2).

### c. Cyclone detection and tracking

Cyclones are identified and tracked using the algorithm introduced by Crawford and Serreze (2016) and modified by Crawford et al. (2021) for use with high-resolution datasets like ERA5. First, sea level pressure data are regridded to a Lambert azimuthal equal-area grid with a resolution of 25 km × 25 km and 100 km × 100 km for ERA5 and MERRA-2, respectively. A grid cell is considered a cyclone center if all following conditions are met:

1) Its SLP is lower than all other grid cells within a 200-km $x$ or $y$ distance.
2) The average SLP difference in a 1000-km radius around the grid cell is at least 7.5 hPa.
3) The grid cell has an elevation less than 1500 m, and the elevation of at least 60% of the grid cells within a 200-km $x$ or $y$ distance is also below 1500 m.

Cyclone area is initially defined by the highest isobar that encloses only the cyclone center in question and no SLP maxima. If merging two cyclones whose centers are within 1200 km at least doubles the size of the larger cyclone, the cyclones are combined into a multicenter system.

Cyclone tracking is conducted every 3 h and has two steps. First, the future position of a storm in the subsequent observation time is predicted based on prior propagation. The cyclone center in the subsequent observation time that is nearest to this predicted location and within 450 km of the current location is considered the best match (implying a maximum propagation speed 150 km $h^{-1}$.)

Results from this algorithm have little sensitivity to spatial resolution of 25 versus 100 km (Crawford et al. 2021). Analysis is only conducted on cyclones that last at least 24 h and travel at least 1000 km. Several storm characteristics are recorded for each 3-h observation, including the central pressure, the local Laplacian of central pressure, and the maximum 925-hPa wind speed within 600 km of the cyclone center [similar to Day et al. (2017)].

Cyclone-associated precipitation (CAP) is calculated following the method of Crawford and Serreze (2017). For each cyclone observation time, the corresponding large-scale precipitation field is divided into contiguous areas for which all grid cells exceed 0.1875 mm (corresponding to a precipitation rate of 1.5 mm $day^{-1}$). This eliminates some trace precipitation, which is typically overestimated in atmospheric reanalyses, especially MERRA-2 (Boisvert et al. 2018). Precipitation areas are associated with a cyclone if 1) they intersect the cyclone's outermost closed isobar or 2) part of the precipitation area is within 250 km of the cyclone center. If a single precipitation area can be associated with multiple cyclones, it is partitioned so that each grid cell in the precipitation area is assigned to the nearest cyclone area. Finally, total precipitation (including convective precipitation) for all associated grid cells is assigned to each cyclone.

### d. The maximum Eady growth rate

The maximum Eady growth rate (EGR) is a measure of baroclinic instability (Eady 1949); it indicates how conducive the environment is to cyclogenesis and deepening (Hoskins and Valdes 1990; Pierrehumbert and Swanson 1995). EGR has two key components: static stability ($N$) and vertical wind shear ($S$):

$$\mathrm{EGR} = 0.3098\,\frac{S}{N}. \tag{1}$$

Static stability is related to the vertical gradient in potential temperature ($\theta$):

$$N = \left(\frac{g}{\theta}\,\frac{\delta\theta}{\delta z}\right)^{0.5}, \tag{2}$$

where $g$ is the acceleration due to gravity and $z$ is the vertical coordinate. The vertical shear of the horizontal wind ($\mathbf{U}$) is

$$S = \left| f\,\frac{\delta \mathbf{U}(z)}{\delta z} \right|, \tag{3}$$

where $f$ is the Coriolis parameter. This is proportional to the horizontal temperature gradient based on the thermal wind equation (Wallace and Hobbs 2006). EGR and its components are calculated every 3 or 6 h for ERA5 and MERRA-2, respectively, using the 925-, 850-, and 700-hPa levels for discrete calculations. We use these low levels because the impact of sea ice loss is most strongly felt in the lower troposphere (Rinke et al. 2006; Serreze et al. 2009).

### e. Comparison of sea ice and cyclone development

Anomalies with respect to the 1981–2010 climatology for each grid cell and day-of-year are calculated for seven environmental variables: SIC, sensible and latent heat fluxes, static stability, vertical wind shear, EGR, and precipitable water. For each cyclone observation, the average anomaly of each variable within a 600-km radius of its center is recorded. Note that the satellite-derived SIC and MERRA-2 EGR

variables have coarser temporal resolution than the cyclone observations. In these cases, multiple consecutive cyclone observations are linked to the same field of SIC or EGR.

Since the goal of this paper is to assess whether variability in SIC can impact Arctic cyclone intensification, we limit our analysis to a "period of interest" for each track, during which the cyclone meets three criteria:

1) its center is over the study area (Fig. 1),
2) less than 20% of the 600-km-radius area around its center lies over land, and
3) it has not yet reached maximum intensity.

Any track for which that period of interest is at least 9 h long is used for statistical analysis (2606 tracks from ERA5 and 3016 tracks from MERRA-2).

Next, a series of linear regression models are constructed using cyclone tracks as the unit of analysis with one of several intensification metrics as the left-hand variable and two right-hand variables: the number of hours in the period of interest ($t$) and the sum of the SIC anomalies experienced by the storm for all hours within that period of interest (i.e., the accumulated SIC anomaly, or $\sum \mathrm{SIC}_a$) [Eq. (4)]:

$$Y = \alpha + \beta_1 t + \beta_2 \sum \mathrm{SIC}_a. \tag{4}$$

Including the number of hours for each track controls for the fact that the more time spent deepening, the more intense a storm is likely to become, regardless of sea ice conditions.

Like using a running 3-month average, a separate regression model is used for each of the twelve 3-month periods. Therefore, "January" refers to pooling all storms December–February, "February" to pooling all storms January–March, and so on. Lagged versions of Eq. (4) are also employed, which incorporate SIC from 3 or 4 days before each cyclone observation instead of SIC on the same day. (This time scale was chosen based on synoptic-scale variations in atmospheric and sea ice activity.)

Intensity is measured in three ways: total deepening (the drop in central pressure during the period of interest), the maximum Laplacian of central pressure, and the maximum 925-hPa wind speed within 600 km of the center. Total deepening ($\Delta p$) is scaled by latitude ($\phi$), following previous studies (e.g., Stewart and Donaldson 1989; Serreze et al. 1997):

$$\Delta p = (p_0 - p_{\min}) \frac{\sin\phi}{\sin 60^\circ}, \tag{5}$$

where $p_{\min}$ is the minimum central pressure observed in the study area and $p_0$ is the initial central pressure. Central pressure and its Laplacian are standard cyclone intensity measures (e.g., Ulbrich et al. 2009; Simmonds and Rudeva 2012; Koyama et al. 2017). Maximum wind speed has been used in multiple recent studies (e.g., Day et al. 2017; Valkonen et al. 2021).

Equation (4) is also used to assess the relationship between SIC and 1) the maximum precipitable water during the period of interest and 2) the total precipitation for the cyclone during or after the period of interest.

To provide context for these sea ice–cyclone relationships, simple linear regression models are also constructed with the average SIC anomaly experienced by cyclones as the lone right-hand variable and the average anomalies of surface sensible and latent heat fluxes, static stability, wind shear, or EGR during the period of interest as the left-hand variable:

$$Y = \alpha + \beta \mathrm{SIC}_a. \tag{6}$$

Because of significant trends in some input variables, statistical models are also constructed using detrended anomalies for Eqs. (4) and (6) (see the online supplemental material).

## 3. Results

### a. Average monthly conditions

Using ERA5 results, cyclone frequency in the study area is greatest in summer (Figs. 2a–c), when the central Arctic Ocean is a relative maximum in both track density (Fig. 2b) and storm intensity (Figs. 2e,h). In winter, storm frequency and intensity are highest on the Atlantic side of the study area and lowest on the Pacific side (Figs. 2a,d,g). The peak intensity of Arctic Ocean cyclones is generally higher in winter than summer. In all months, the Arctic Ocean is primarily a region of cyclone filling and dissipation (negative deepening; Figs. 2j–l), although cyclone deepening (positive values) is more common in warmer months (May–September). MERRA-2 results yield the same seasonality (Fig. S3).

The theoretical basis for SIC influencing Arctic Ocean cyclones starts with reduced SIC enhancing upward sensible and latent heat fluxes to the atmosphere. Heating the lower atmosphere reduces static stability, making an environment more suitable for cyclone development. Just as cyclone intensity exhibits seasonality, so too do SIC, surface heat fluxes, and (in)stability variables (Fig. 3). Because the focus of this study is the connection between SIC variability and cyclone intensification, monthly averages for these variables are calculated only within 600 km of cyclones deepening over the Arctic Ocean. Using all cyclone observations yields nearly identical results except for wind shear and EGR, which are weaker in all months (Fig. S4).

The average sensible heat flux is consistently downward (negative) in July and August under deepening cyclones (Fig. 3b). It may average upward or downward depending on the year in other months, although upward sensible heat fluxes are more common from October to May, when SIC is increasing or generally above 90% (Fig. 3a). The latent heat flux is consistently upward in all months, but notably weaker in January–March (Fig. 3c).

The seasonality of low-level (925–700 hPa) static stability is opposite the seasonality of latent heat fluxes (Fig. 3d). The lower atmosphere is most stable from January to March, when latent heat fluxes are lowest. Static stability is lowest in June, when latent heat fluxes are greatest but sensible heat fluxes are more often downward. The seasonality of the vertical shear of horizontal wind matches closely with static stability: Wind shear is higher in winter and lower in summer (Fig. 3e). As shown in Eq. (1), these two factors counteract

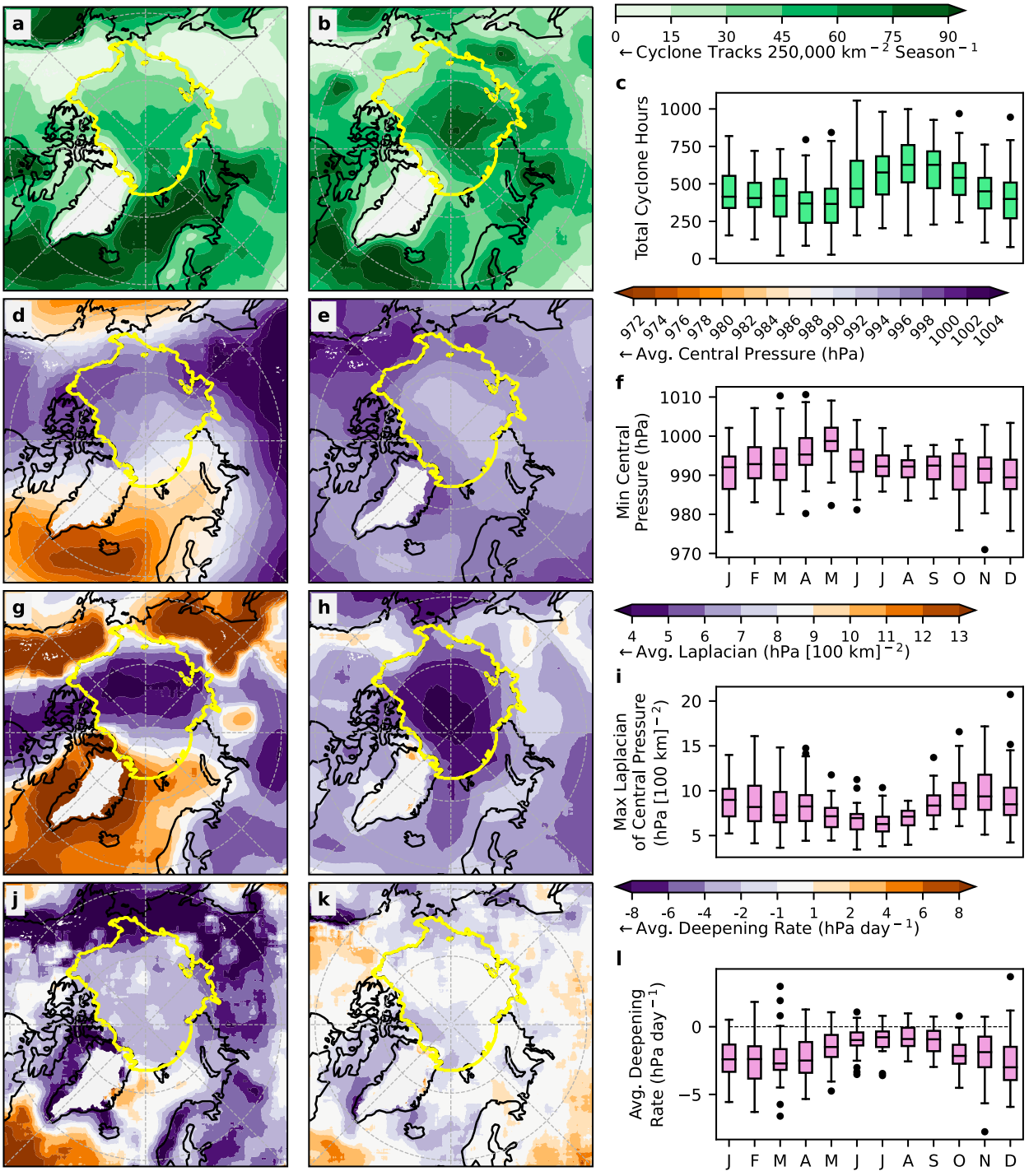


FIG. 2. (left),(center) Climatology (1981–2010) of (a),(b) cyclone frequency, (d),(e) cyclone central pressure, (g),(h) Laplacian of central pressure, and (j),(k) pressure tendency in (left) winter (DJF) and (center) summer (JJA) spatial distribution. (right) Boxplots of (c) total cyclone hours each month (number of cyclones × average cyclone lifespan), and monthly averages of each cyclone's (f) minimum central pressure, (i) maximum Laplacian of central pressure, and (l) average deepening rate for cyclones within the study area (yellow outline in maps). All boxes span the interquartile range, with the horizontal line indicating the median, the whiskers extending to the most extreme values within 1.5 times the interquartile range, and dots indicating outliers beyond 1.5 times the interquartile range. All data are derived from ERA5.

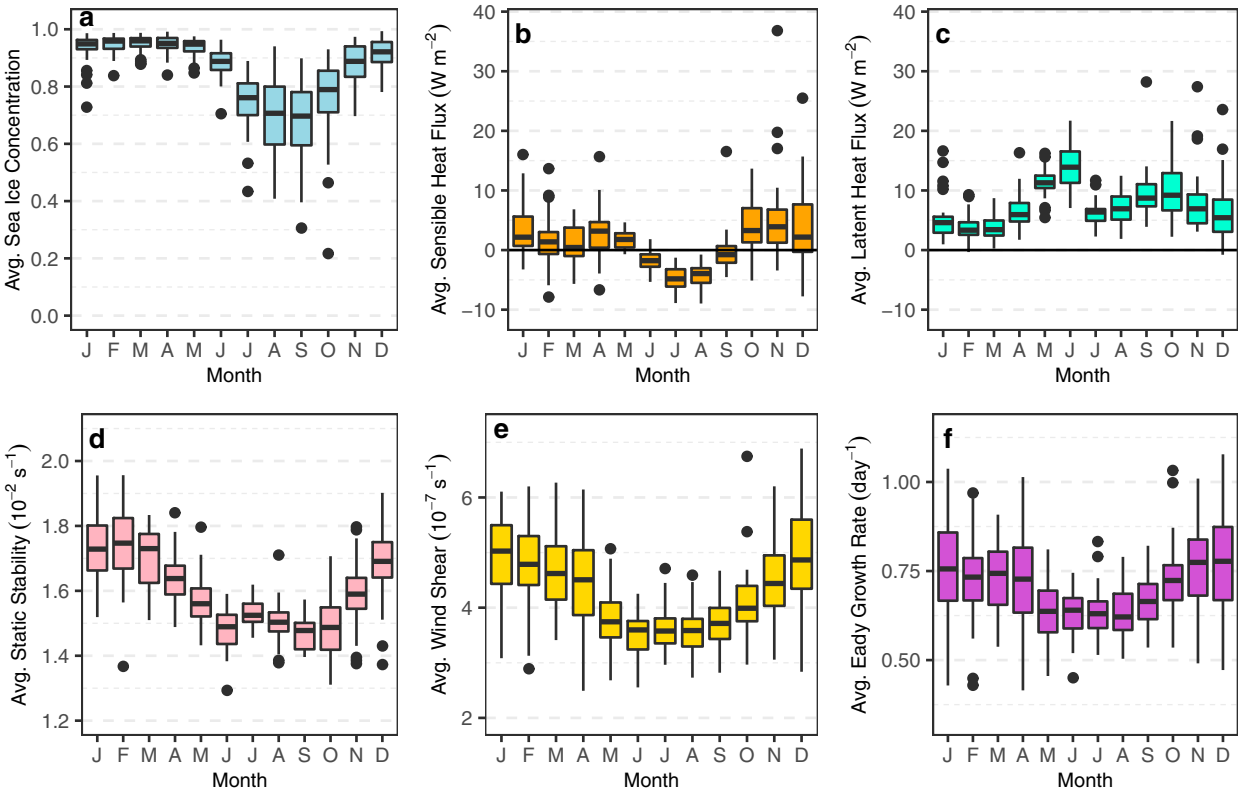


FIG. 3. Boxplots of average environmental conditions experienced by cyclones that are deepening over the Arctic Ocean study area (ERA5; 1979–2019), including (a) SIC, (b) surface sensible heat flux, (c) surface latent heat flux, (d) static stability, (e) vertical shear of horizontal wind, and (f) EGR. Turbulent fluxes are positive upward. EGR and its components are calculated for 925–700 hPa. All boxes span the interquartile range, with the horizontal line indicating the median, the whiskers extending to the most extreme values within 1.5 times the interquartile range, and dots indicating outliers beyond 1.5 times the interquartile range.

each other, so there is less seasonality in EGR than either of its components (Fig. 3f).

Figure 3 uses data from ERA5. Using MERRA-2 instead yields very similar results for static stability, wind shear, and EGR (Fig. 4). However, except for during June–August, average sensible heat fluxes are substantially greater in MERRA-2 than in ERA5. From October to April, monthly average sensible heat flux under deepening cyclones is 10–20 W m$^{-2}$ upward in MERRA-2 but only 0–5 W m$^{-2}$ in ERA5. Still, sensible heat fluxes follow a similar seasonality of upward in winter and downward in summer.

### b. *Lifespan of the average cyclone*

Cyclones within the study area (Fig. 1) exhibit their fastest deepening rates at the beginning of their lifespans (Fig. 5a). Deepening decelerates until minimum pressure is reached. This phase accounts for 29% of the average storm's lifespan in winter (40% in summer). This is followed by cyclone filling until the storm dissipates at the end of its lifespan. This pattern is typical of extratropical cyclones reacting to the top-down influence of the polar jet stream (Thorncroft et al. 1993; Hoskins and Hodges 2019) and/or tropopause polar vortices (Tanaka et al. 2012; Simmonds and Rudeva 2014; Aizawa and Tanaka 2016). Since the bottom-up influence of SIC variability is only expected to modify this typical U-shaped pressure curve, we focus only on the deepening phase.

The majority of Arctic Ocean cyclones migrate into the study area from more southerly genesis regions (Crawford and Serreze 2016; Aizawa and Tanaka 2016). Therefore, the average SIC experienced by cyclones entering the study area (e.g., from the Greenland Sea or Barents Sea) is typically lowest when the storms are youngest (Fig. 5b), and therefore intensifying most quickly. Similarly, surface turbulent heat fluxes, wind shear, and EGR influencing these cyclones all tend to be strongest at cyclogenesis and weaker at the point of cyclolysis (Figs. 5c–f). Results from MERRA-2 are comparable to those from ERA5 except for the sensible heat flux being greater in winter and the SIC being lower in both seasons (Fig. S5).

Although these results suggest a negative correlation between SIC and storm deepening (as theorized), the correlation may be coincidental because 1) SIC is typically higher at higher latitudes, 2) many Arctic storms have poleward trajectories, and 3) storms typically deepen when they are younger then dissipate as they age. We remove the dependence of SIC, surface fluxes, and (in)stability fields on latitude and seasonality by conducting the following analysis using their anomalies relative to a given grid cell and day of year.

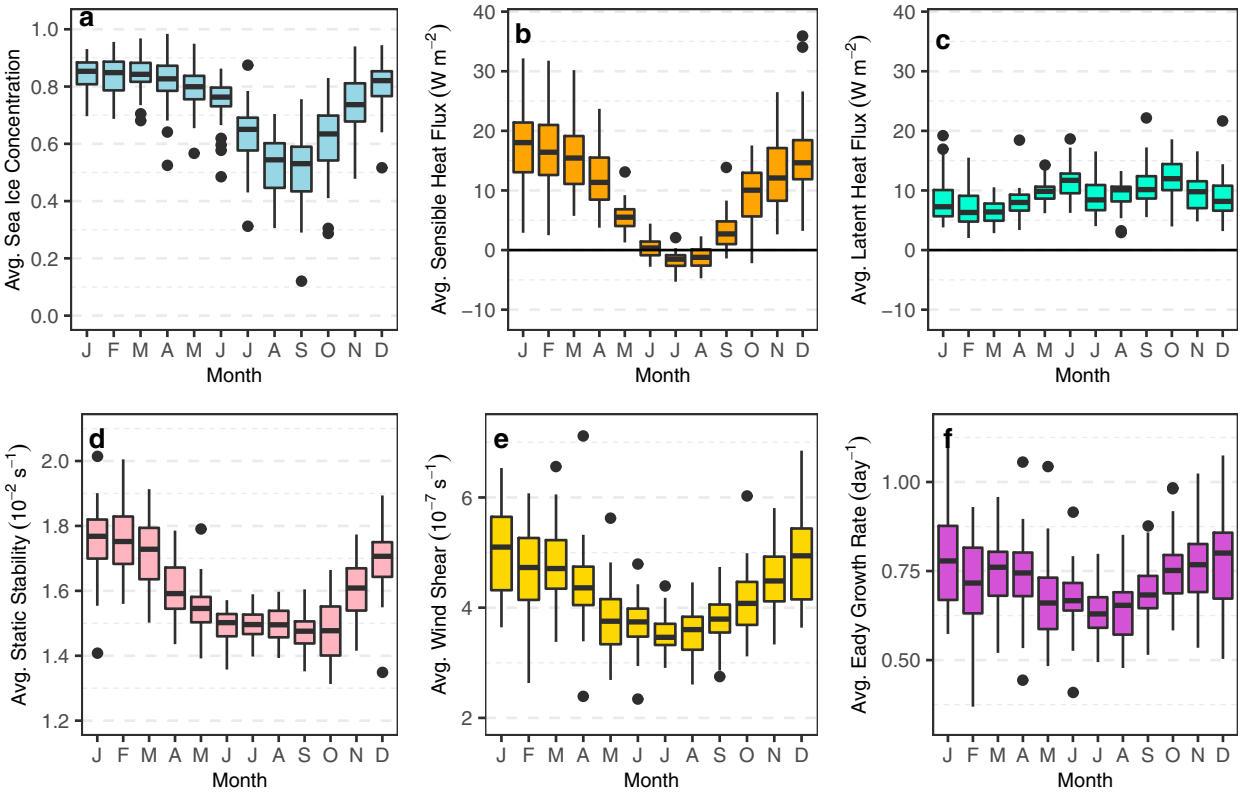


FIG. 4. As in Fig. 3, but using data from MERRA-2.

*c. Sea ice concentration and storm intensity*

To visualize how SIC anomalies and storm intensification are compared, consider February storms whose period of interest lasts exactly 27 h (Fig. 6). This subset was chosen to illustrate our methods because it exhibits instances of both positive and negative accumulated SIC anomalies and contains storms with a wide range of genesis locations. The entire length of each cyclone track is plotted in Fig. 6a. The period of interest (red lines) for each track is when 1) the storm is deepening, 2) its center lies within the study area and 3) the area with a 600-km radius centered on the storm comprises less than 20% land. Only that period of interest is used to calculate the values in Fig. 6b. For example, track 140 lasted several days, migrating north from the Bering Sea, but the average SIC anomaly (within a 600-km radius) is only calculated for the 27 h within the period of interest. The sum of those anomalies yields the accumulated SIC anomaly $\left(\sum \mathrm{SIC}_a\right)$. Other measures of storm intensity are also summarized, and this process is repeated for each of thousands of cyclone tracks.

For each 3-month period and each reanalysis, a linear regression model [Eq. (4)] was then constructed with cyclone deepening of each track as the left-hand variable and two right-hand variables: 1) the number of hours in the period of interest ($t$) and 2) the accumulated SIC anomaly $\left(\sum \mathrm{SIC}_a\right)$. The ERA5 results for January storms are presented in Fig. 7a. The colored shading shows how many storms had each combination of deepening hours ($x$ axis) and accumulated SIC anomaly ($y$ axis). About 43% of all observed tracks experience an accumulated SIC anomaly between −25% and 25%; about 17% of tracks experience below −75% accumulated SIC anomaly; and only about 6% of tracks experience above +75%. This asymmetry is related to the average SIC in January exceeding 90%. (Since the maximum possible anomaly for any one hour is +10%, the maximum SIC anomaly over a 12-h span is only +120%.)

The regression results appear as slanted contour lines. If the accumulated SIC anomaly is 0% (i.e., normal sea ice conditions), then the predicted deepening for a storm lasting 24 h is about 6.2 hPa. This represents the median storm for ERA5 in January (Table S1). If the accumulated SIC anomaly is held constant at 0%, then increasing the period from 24 to 36 h will lead to a predicted deepening of 8.4 hPa. This is intuitive: The longer a storm spends intensifying, the more intense it can get. If length of time is held constant at 24 h but the accumulated SIC anomaly is changed from 0% to −250% (i.e., an average anomaly of about −10% for 24 h), the predicted deepening is about 9.0 hPa. In other words, January storms tend intensify more if they pass over anomalously low SIC (negative anomalies) as opposed to anomalously high SIC (positive anomalies).

More precisely, the effect of SIC variability on storm intensification is given by the regression coefficient for accumulated SIC anomaly [$\beta_2$ in Eq. (4)], which is $-1.1\,\mathrm{hPa}\left(\sum \mathrm{SIC}_a\right)^{-1}$. This means that for an accumulated SIC anomaly of −75%, a

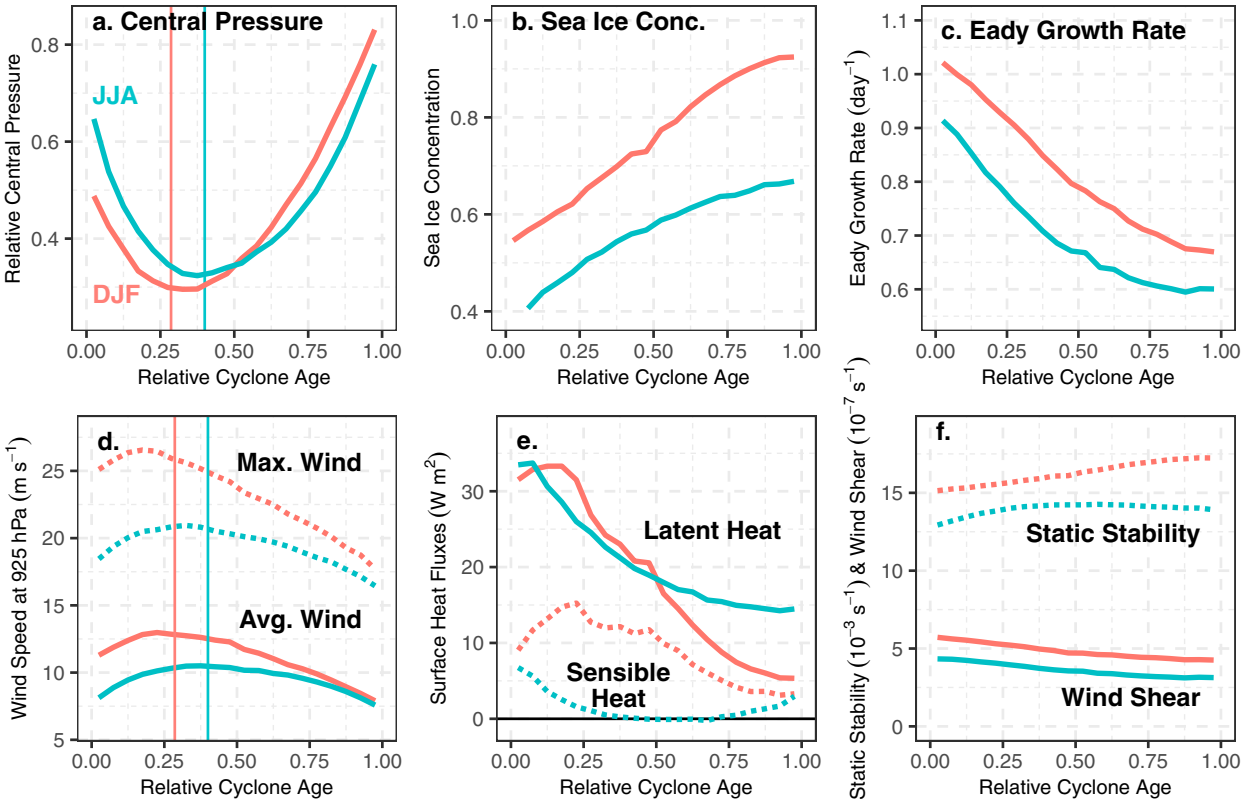


FIG. 5. Average conditions experienced by Arctic Ocean cyclones relative to cyclone age, including (a) relative central pressure (1 = maximum, 0 = minimum), (b) SIC, (c) EGR, (d) maximum and average 925-hPa wind speed, (e) surface sensible and latent heat fluxes (positive upward), and (f) static stability and wind shear. Averages are calculated separately for winter (red) and summer (teal). Vertical lines in (a) and (d) mark the average age at which cyclones experience minimum pressure. All averages calculated with ERA5.

storm in January will experience additional deepening of 0.8 hPa, or 12.9% more than the median deepening. About one in six January cyclones in this study experience an accumulated SIC anomaly exceeding −75% (Fig. 7a). Contrast the situation for January storms with October storms, for which the contours are almost perfectly vertical (Fig. 7b). Vertical contours indicate that the accumulated SIC anomaly has no impact on deepening for this period; only an increase in the period of interest leads to more deepening.

Because of space constraints, the regression models for the remaining 3-month periods for ERA5 and MERRA-2 are summarized using just that coefficient [$\beta_2$ in Eq. (4)] for the accumulated SIC anomaly (Fig. 8a; see Table S2 for additional coefficients). Negative coefficients for accumulated SIC anomaly indicate that negative SIC anomalies are associated with more cyclone intensification (i.e., more deepening, a greater pressure drop). Significant negative relationships exist for December–June using ERA5. These same months (minus April) also show significant negative relationships using MERRA-2. In general, reduced SIC is predictive of greater cyclone intensification in winter and most spring months, but not summer or early autumn.

Coefficients for winter months remain significant using a 3-day lag (Fig. 8b) or 4-day lag (Fig. S6), strengthening the evidence that variability in SIC has an influence on cyclone intensification. When applying modifications to the methodology, such as changing the aggregation radius (Fig. S7), using the NASA Team algorithm for SIC (Fig. S8), or using detrended SIC and intensity values (Fig. S9), we still see a significant inverse relationship between SIC anomaly and cyclone intensification in winter and no relationship in summer or autumn. However, sea ice conditions have a stronger relationship to cyclone deepening for storms that migrate into the study region compared to those that are generated locally (Fig. S10), especially in March.

Coefficients for April–June are less robust than those for December–February, with fewer significant lagged relationships (Fig. 8b) and more sensitivity to search radius (Fig. S7), sea ice data source (Fig. S8), and genesis location (Fig. S10). Therefore, evidence for SIC variability impacting storm development is weaker for spring than for winter.

Central pressure is not the only measure of storm intensity, so Eq. (4) was also examined using the maximum Laplacian of central pressure (Figs. 8c,d) and maximum 925-hPa wind speed (Figs. 8e,f). With no time lag, significant negative coefficients exist for both metrics and reanalyses in December–March and at least one reanalysis/metric in November and April–June. By contrast, the July–October period still shows no significant inverse relationships. The greatest relative magnitude for the wind coefficients is 7% of median maximum

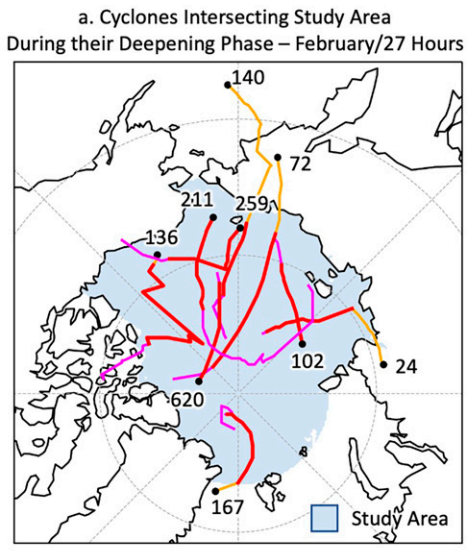


b. Statistics for Period of Interest (red lines in map)

| # | Year | $\Delta p$ hPa | $\nabla^2 p_{max}$ * | $U_{max}$ m/s | CAP kg/m² | $\Sigma$SICa % |
|---|---|---|---|---|---|---|
| 259 | 2018 | 4.1 | ***24.4*** | 20.9 | 0.43 | **52.9** |
| 211 | 2019 | ***0.1*** | ***21.5*** | 26.2 | 0.54 | **39.1** |
| 72 | 2014 | **12.3** | 64.8 | **38.9** | **0.65** | **18.8** |
| 620 | 2018 | 6.7 | 53.4 | **37.0** | 0.45 | 9.3 |
| 102 | 1980 | 8.1 | 30.3 | **30.1** | ***0.30*** | -10.7 |
| 24 | 2008 | 3.9 | ***19.2*** | ***14.2*** | ***0.28*** | -12.4 |
| 136 | 1998 | **14.1** | 34.6 | 20.8 | 0.35 | -23.1 |
| 140 | 1989 | 2.1 | 52.2 | **30.5** | 0.46 | -26.7 |
| 167 | 1983 | **20.6** | **103.2** | **35.9** | **0.62** | ***-69.7*** |

*Units are $\frac{hPa}{[100\ km]^2}$

**Bold** = Above 75th percentile
***Bold Italics*** = Below 25th percentile

Local Genesis  Remote Genesis

FIG. 6. (a) Map of all cyclone tracks intersecting the study area during their deepening phase for exactly 27 h in any February 1979–2019. The total deepening ($\Delta p$) for storms is calculated only for the part of tracks (red color) 1) that are within the study area (light blue shading) and 2) for which less than 20% of the area within 600 km of the cyclone center is masked as land. (b) Total deepening ($\Delta p$), maximum Laplacian of central pressure ($\nabla^2 p_{\max}$), maximum wind speed ($U_{\max}$), total CAP, and accumulated SIC anomaly $\left(\sum \mathrm{SIC}_a\right)$ during the valid part of the deepening phase (red lines on map; i.e., the period of interest). Values above the 75th percentile for February 1979–2019 are in boldface. Values below the 25th percentile for February 1979–2019 are in boldface and italics. All data from ERA5.

925-hPa wind speed per 100% accumulated SIC anomaly in March (using either reanalysis). Compared to total deepening, the relationships for these local instantaneous metrics are more sensitive to time lags, but significant inverse relationships persist for both metrics and reanalyses in January–March. Like the pattern observed for total deepening, there is strong evidence that reduced SIC leads to greater storm intensification in winter and weaker evidence for this relationship in spring.

### d. *Sea ice concentration and cyclone moisture*

In addition to pressure and wind, cyclone-associated precipitation is another measure of storm intensity. Also using Eq. (4), total precipitation and maximum precipitable water were compared to SIC anomalies (Fig. 9). November–May exhibit a significant relationship between the accumulated SIC anomaly and CAP using either reanalysis. All significant coefficients are negative, meaning that reduced SIC correlates with greater atmospheric moisture and more CAP. Similar to findings for wind speed, the greatest relative magnitude coefficient is 12% of median CAP in March per 100% accumulated SIC anomaly for ERA5 (8% for MERRA-2). Compared to the cyclone intensification results, the relationship between the accumulated SIC anomaly and CAP is less impacted by using SIC from three days prior to the cyclone observations. Notably, though, every month (even summer and autumn months) yields significant negative relationships with a 3-day lag between maximum precipitable water and accumulated SIC anomaly. Using SIC from the NASA Team algorithm (Fig. S11) or using detrended inputs (Fig. S12) yields consistent results.

### e. *Physical mechanisms for sea ice influence on storm intensification*

The theory behind SIC influencing storm development has two key steps. First, if the sea ice barrier between the ocean and atmosphere is removed, surface sensible and latent heat fluxes may increase (Royer et al. 1990; Schweiger et al. 2008; Bader et al. 2011). Second, this addition of heat to the lower atmosphere reduces static stability, making the environment more favorable for cyclone development (Bader et al. 2011; Jaiser et al. 2012). Reduced static stability also can enhance wind speed more generally (Seo and Yang 2013; Mioduszewski et al. 2018).

To assess these links, we compared the anomalies in latent and sensible heat flux, static stability, the vertical shear of horizontal wind, and EGR to SIC anomalies within 600 km of each cyclone observation and then averaged these anomalies for the period of interest of each cyclone track. These data were then input to Eq. (6). Results show significant negative correlations between EGR and SIC for both reanalyses in December–April (Fig. 10a). This means that reduced sea ice cover makes the environment more conducive to cyclone development in colder months. Coefficients for June–October

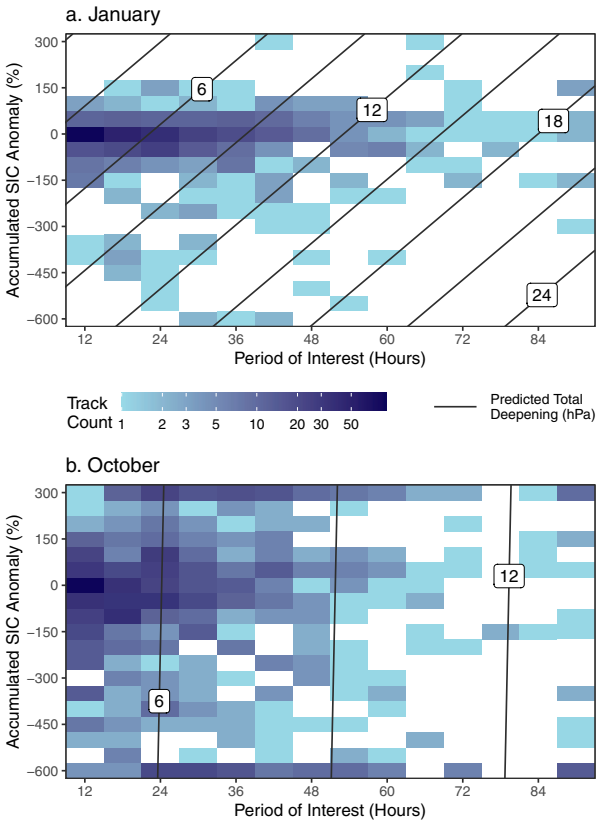


FIG. 7. 2D histograms of the accumulated SIC anomaly vs the hours in the period of interest for storms over the study area (shading) overlain by the predicted total deepening based on Eq. (4) using ERA5 storm tracks and no time lag. Bins along the top, right, and bottom edge include cyclone tracks that exceed the plot boundaries. Data are from 3-month periods centered on (a) January and (b) October.

are weaker, and although significant in August/September for MERRA-2, these coefficients have a positive sign, indicating that, if it has any impact, reduced SIC makes the environment less conducive to cyclone development in late summer.

Separating EGR into its two components reveals how its relationship with sea ice is mostly driven by a positive relationship between SIC and static stability (Fig. 10b). Significant coefficients exist for September–April; however, the coefficients for September/October are weak (<2% of mean static stability per 10% SIC change, respectively) compared to December–April (3%–8% of mean static stability per 10% SIC change). Coefficients are also consistently greater in ERA5 than MERRA-2.

However, extratropical cyclones are more likely to develop not only if static stability is weak, but also if vertical shear of horizontal wind is strong [Eq. (1)]. Vertical wind shear (Fig. 10c) is greater with reduced SIC in December–February for both reanalyses. Weaker static stability and stronger wind shear both facilitate greater EGR, so the influence of SIC on each component is reinforcing in winter. However, reduced sea ice in September/October yields counteracting effects on EGR, weakening static stability but also slightly weakening vertical wind shear. Therefore, sea ice reductions best facilitate storm intensification when reducing sea ice both 1) significantly weakens static stability and 2) simultaneously strengthens vertical wind shear. That combination only occurs in winter, the same season for which the accumulated SIC anomaly has a significant relationship with all three intensity metrics (Fig. 8).

The seasonality of the sea ice–static stability relationship can be traced to the impact of SIC on the surface turbulent heat fluxes (Figs. 10d,e). The sensible and latent heat fluxes have significant (albeit negative) relationships with SIC from September to March (plus April for latent heat) for both reanalyses. As with static stability, the coefficients are strongest in winter and stronger in ERA5 than MERRA-2. Since fluxes are positive upward, a negative relationship means that reducing SIC leads to greater upward turbulent heat fluxes. The lack of relationship between SIC variability and these surface heat fluxes in summer translates to the lack of relationship between SIC variability and summer cyclone development. Note that summer is also the season when the average sensible heat flux is downward (Figs. 3 and 4).

## 4. Discussion

### a. *Comparison to past work*

The hypothesis that large sea ice anomalies at the end of summer should impact autumn/winter cyclone activity has appeared in several studies, but results from tests of this hypothesis have been mixed. With no relationship found in September–November, our results are consistent with Koyama et al. (2017) but inconsistent with Simmonds and Keay (2009). The contrast between significant relationships in winter and no relationship in summer/autumn is consistent with Valkonen et al. (2021). Our result finding that precipitable water and CAP both increase in response to negative accumulated SIC anomalies is consistent with past work showing increased CAP associated with low seasonal SIC (Finnis et al. 2007; Stroeve et al. 2011; Crawford and Serreze 2017).

One limitation of several prior studies is that, when examining seasonal anomalies of SIC and cyclone activity, it is difficult to disentangle sea ice influencing cyclone development from cyclones both thermodynamically and mechanically influencing the sea ice cover (Deser et al. 2000; Bader et al. 2011; Valkonen et al. 2021). By focusing on the intensification of individual cyclone tracks in relation to daily (or subdaily) SIC anomalies instead of the average intensity of all storms in a season, we provide stronger evidence that exposure to negative SIC anomalies causes storms to experience greater intensification in winter (and possibly spring), but not in summer or early autumn. The winter relationship still holds when SIC from three or four days prior to cyclone observations is used instead of same-day SIC. This further supports the idea that reduced SIC is not simply correlated with greater storm intensity; it also causes greater storm intensification.

Our result that reducing SIC leads to greater upward turbulent heat fluxes is consistent with previous work (Royer et al. 1990; Koyama et al. 2017). Similarly, the lack of significant

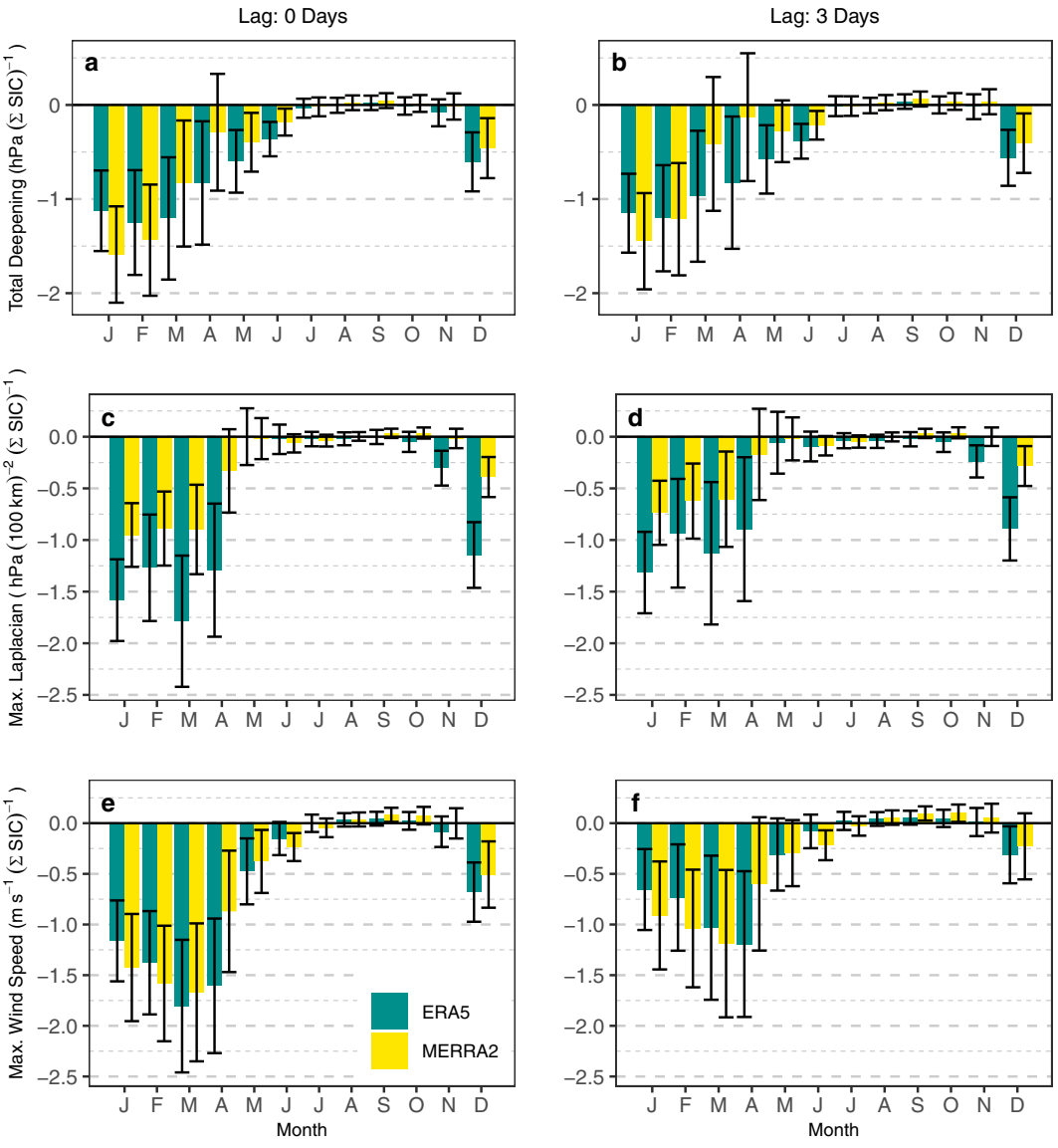


FIG. 8. Regression coefficients for the accumulated SIC anomaly in the Eq. (4) regression models with a left-hand variable of (a),(b) the total deepening for a cyclone in its period of interest, (c),(d) the maximum Laplacian of central pressure experienced by a cyclone, and (e),(f) the maximum 925-hPa wind speed experienced by a cyclone. A separate regression model is constructed for each month and reanalysis, and models are constructed using both the SIC anomalies (left) for the same day as and (right) 3 days before each 3-h cyclone observation. Error bars indicate the 95% confidence interval for coefficients.

negative coefficients in May–August (and even some significant positive coefficients) is consistent with the literature describing Arctic amplification of warming as a primarily a cold-season phenomenon (Rinke et al. 2006; Serreze et al. 2009). However, the decomposition of EGR into static stability and vertical wind shear in this study provides a novel perspective on the sea ice–cyclone relationship that helps explain the difference in results from Koyama et al. (2017), who focused on September–November, versus Valkonen et al. (2021), who focused on December–May. Although September and October have witnessed some of the largest SIC variability in recent decades, the impact of negative SIC anomalies in these months is to somewhat weaken both static stability and vertical wind shear. The consequence for cyclone intensification is that these two tendencies effectively cancel each other out, and cyclones are insensitive to SIC variability. In winter, on the other hand, negative SIC anomalies substantially weaken static stability while strengthening vertical wind shear. These reinforcing tendencies lead a significant influence of SIC variability on storm intensification. Therefore, Koyama et al. (2017) detected no clear relationship between SIC variability and storm intensity in fall, but Valkonen et al. (2021) did find such a relationship in winter and spring.

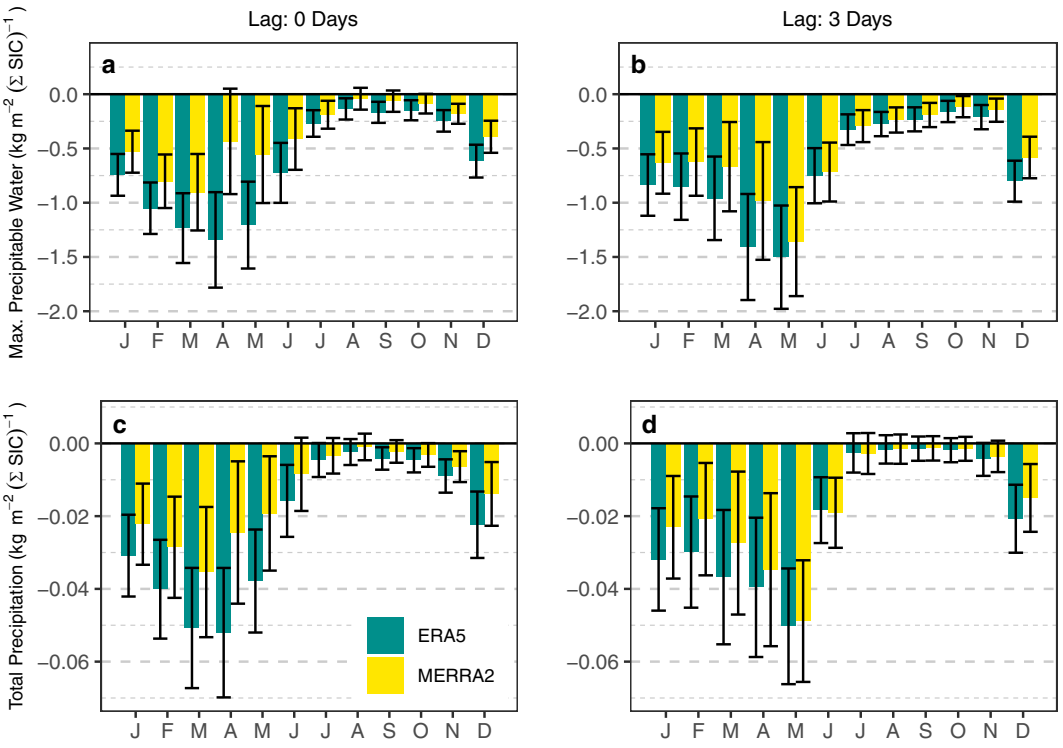


FIG. 9. Regression coefficients for the accumulated SIC anomaly in the Eq. (4) regression models with a left-hand variable of (a),(b) the maximum total precipitable water experienced by a cyclone and (c),(d) the total precipitation generated by a cyclone. A separate regression model is constructed for each month and reanalysis, and models are constructed using both the SIC anomalies (left) for the same day as and (right) 3 days before each 3-h cyclone observation. Error bars indicate the 95% confidence interval for coefficients.

Why does reduced sea ice lead to stronger wind shear in winter months but slightly weaker wind shear in September and October? Low-level vertical wind shear is proportional to the horizontal temperature gradient near the surface. In winter, the sea ice surface is much colder than adjacent open ocean, which can enhance wind shear and EGR locally (Bader et al. 2011), and the study area typically exceeds 90% SIC (Figs. 1a,c). Observations from leads in sea ice show that even small reductions in winter SIC lead to large upward turbulent heat fluxes (Walter et al. 1995; Raddatz et al. 2012). Therefore, reduced SIC in winter has the potential to encourage stronger horizontal temperature gradients. In September and October, mean SIC is much lower (Fig. 1c), so a negative anomaly in SIC often reflects a shift from a consolidated ice pack with a distinct edge to a more mixed ice–ocean surface or (in recent years) uniform open water. Such changes reduce horizontal temperature gradients, and therefore wind shear and EGR. Finally, the seasonality of EGR aligns more closely with the seasonality of wind shear than static stability (Fig. 3), so even weak relationships between SIC and wind shear may be more important to cyclone intensification than counteracting relationships between SIC and static stability.

In addition to being a mechanism by which reduced sea ice enhances storm intensity, the latent heat flux also likely contributes to increased CAP. Past work has demonstrated the primary importance of thermodynamic change (i.e., increased saturation vapor pressure) over dynamic change (e.g., increased storm intensity) in driving increased Arctic CAP under global warming scenarios (Cassano et al. 2007; Yettella and Kay 2017). Consistent with these findings, SIC variability has a significant influence (with both reanalyses) on CAP in November and April despite no simultaneous significant impact on cyclone deepening. However, note that no significant relationship between SIC and CAP exists in September or October using MERRA-2, when reduced SIC enhances the latent heat flux but has no impact on storms (Fig. 10e). Additionally, a significant negative relationship between SIC and CAP (Fig. 9c) exists in May without a corresponding relationship between SIC and the latent heat flux. The relationship between SIC variability and storm intensity may explain some of these discrepancies; however, our research framework cannot fully distinguish thermodynamic versus dynamic or local versus remote effects on CAP.

### b. *Study limitations*

One limitation to assessing track-by-track relationships between SIC and storm intensification is that the passive microwave record has a 2-day resolution for 1979–87 and a daily resolution thereafter. The period of interest for a storm often lasts less than 2 days, so there may be only one satellite sea ice observation for the entire period. Although available at a 3-h temporal resolution, the SIC inputs for both MERRA-2

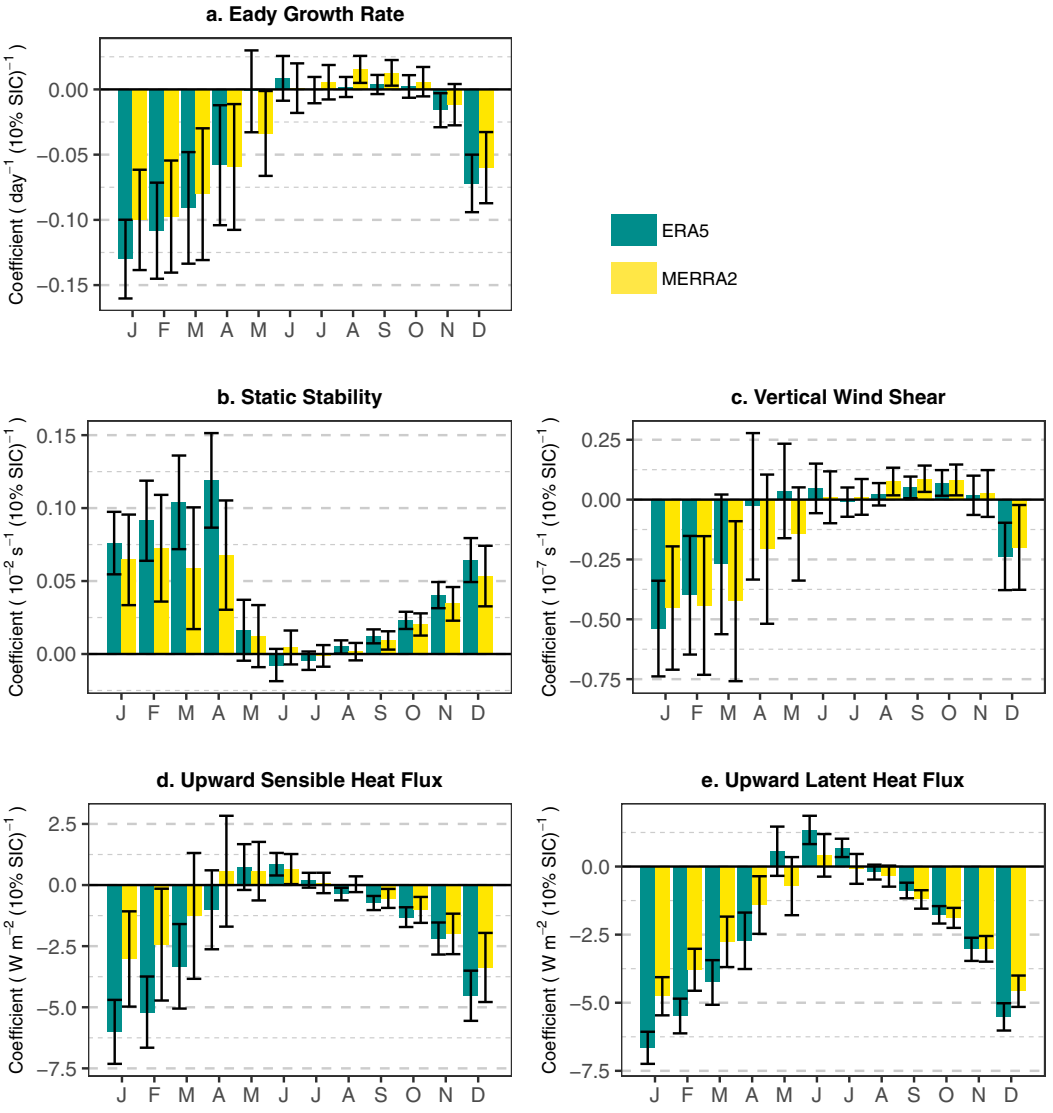


FIG. 10. Regression coefficients for the average SIC anomaly in the Eq. (5) regression models with a left-hand variable of (a) Eady growth rate, (b) static stability, (c) vertical wind shear, (d) surface sensible heat flux, and (e) surface latent heat flux. A separate regression model is constructed for each month and reanalysis. Error bars indicate the 95% confidence interval for coefficients.

and ERA5 are largely derived from this passive microwave record. Using only years with daily SIC does not substantially change results (Figs. S13 and 14). Retrievals of SIC are also affected by clouds and water vapor (Comiso et al. 1997), which are more prevalent under cyclonic conditions, but using a different SIC data source does not substantially change results (Figs. S8 and S11).

As described in section 2a, reanalysis-derived surface turbulent heat fluxes are less reliable than other parameters over mixed sea ice/ocean grid cells (Graham et al. 2019b; Renfrew et al. 2021). MERRA-2 SIC is consistently lower than ERA5 SIC and MERRA-2 sensible heat fluxes are higher, especially in winter (Fig. 3 vs Fig. 4). Consistent differences are observable in the magnitude of coefficients relating SIC variability to surface heat fluxes, but ERA5 and MERRA-2 show general agreement in the seasonality and significance of relationships (Fig. 10). Moreover, despite bias in MERRA-2 SIC, the two reanalyses mostly agree regarding the seasonal relationship between SIC variability and storm intensification.

The linear regression method used provides imperfect control on other variables in the climate system. Although a direct connection whereby reduced SIC enhances cyclone intensification is clear in winter, spring months exhibit substantial uncertainty. Remote impacts on Arctic storm activity, like the poleward shift of the Pacific storm track and weakening of the Atlantic storm tracks, may impact Arctic cyclone activity as well (Akperov et al. 2019; Song et al. 2021). These issues might be better explored by controlled perturbation

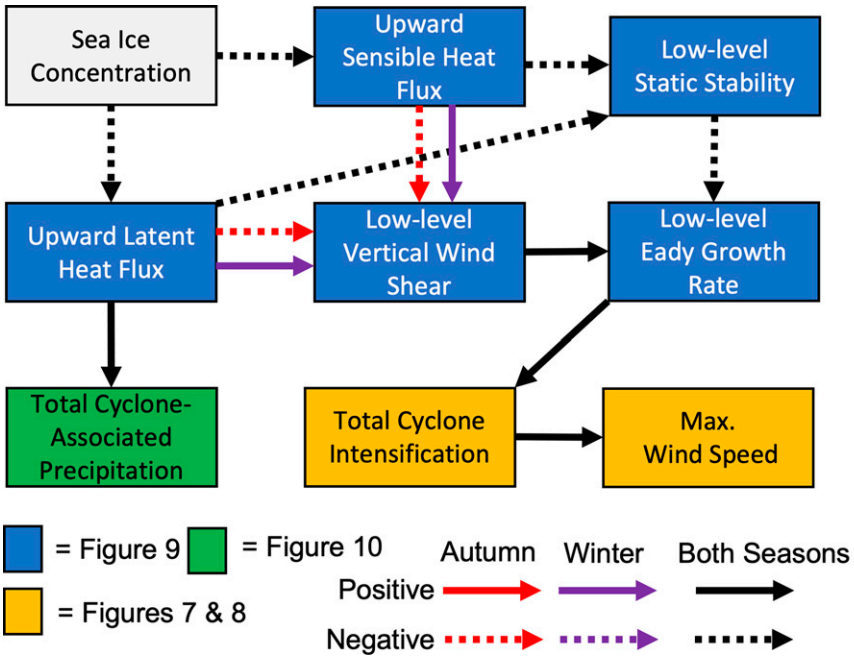


FIG. 11. Conceptual model of the relationships described in this manuscript for early autumn (September–October) and winter (December–March) seasons. Arrow style indicates the sign of the correlation between each pair of variables, and arrow color indicates the relevant season(s). The box color for each variable indicates the figure in which its relationship with sea ice is shown.

experiments in a fully coupled climate model (e.g., Smith et al. 2019).

Finally, this research employs the same cyclone detection and tracking algorithm as two related studies (Koyama et al. 2017; Valkonen et al. 2021). Different algorithms yield broadly comparable results for hemisphere-wide statistics (Neu et al. 2013), especially for the most intense cyclones (Simmonds and Rudeva 2014), but they can differ greatly for some areas, including the Arctic Ocean in summer (Neu et al. 2013; Rohrer et al. 2020; Vessey et al. 2020). Therefore, examining these same questions with additional cyclone detection and tracking algorithms would be valuable.

## 5. Conclusions

Previous studies that examined whether sea ice variability influences Arctic cyclone intensity have provided mixed results and limited ability to prove cause and effect. By measuring all variables at a daily (or finer) scale, we were able to examine multiday lag times between SIC anomalies and cyclone characteristics. We also used individual cyclone tracks, not seasonal averages, as our unit of analysis. These factors allow us to better assess causation. We found strong evidence that sea ice variability impacts cyclone intensification in winter (December–March), weak evidence in spring (April–June), but no evidence in summer or early autumn (July–October).

Incorporating surface energy fluxes and both static stability and vertical wind shear into the study framework provides a richer illustration of why such seasonality exists (Fig. 11). In fall, winter, and early spring, negative SIC anomalies enhance the upward turbulent heat fluxes, weakening static stability. However, only in winter is reduced sea ice also associated with greater low-level (925–700 hPa) vertical wind shear. Weaker static stability and stronger wind shear both enhance baroclinic instability, and therefore cyclone intensification. This leads to stronger maximum cyclone intensity. Reduced SIC also enhances precipitable water and CAP, although our framework does not clearly decompose the importance of storm intensity versus the direct impact of local latent heat fluxes or large-scale moisture transport.

Several previous studies into sea ice impacts of cyclone activity have focused on September, when declines in SIC have been greatest (Stroeve et al. 2011; Koyama et al. 2017). However, reduced SIC in autumn tends to weaken vertical wind shear, counteracting the coincident weakening of static stability. This explains why Koyama et al. (2017) found no significant links between September SIC and September–November storm intensity, whereas Valkonen et al. (2021) found that reduced SIC correlates with stronger storms for the December–May cold season. As winter Arctic SIC continues to decline, our results suggest that more powerful storms that generate stronger winds and more precipitation may be expected in the Arctic. However, this relationship is dependent on the impact of sea ice variability on both static stability and vertical shear of horizontal wind.

*Acknowledgments.* This work was supported by the Canada-150 and Canada Excellence Research Chair (CERC) programs. Support was also provided by the Canada Research Chair

(CRC) and the Natural Sciences and Engineering (NSERC) research council. This work is a contribution to the Arctic Science Partnership and ArcticNet.

*Data availability statement.* ERA5 data are available at https://doi.org/10.24381/cds.adbb2d47. SIC data from the NASA Team algorithm are available at https://doi.org/10.5067/8GQ8LZQVL0VL. MERRA-2 data are available at https://doi.org/10.5067/7MCPBJ41Y0K6 (surface heat fluxes, precipitation, SIC), https://doi.org/10.5067/3Z173KIE2TPD (sea level pressure, total precipitable water), and https://doi.org/10.5067/A7S6XP56VZWS (wind, temperature, geopotential height). Code for the cyclone detection and tracking algorithm can be found at https://doi.org/10.5281/zenodo.4356161.

## REFERENCES


Aizawa, T., and H. L. Tanaka, 2016: Axisymmetric structure of the long lasting summer Arctic cyclones. *Polar Sci.*, **10**, 192–198, https://doi.org/10.1016/j.polar.2016.02.002.

Akperov, M., and Coauthors, 2019: Future projections of cyclone activity in the Arctic for the 21st century from regional climate models (Arctic-CORDEX). *Global Planet. Change*, **182**, 103005, https://doi.org/10.1016/j.gloplacha.2019.103005.

Alexander, M. A., U. S. Bhatt, J. E. Walsh, M. S. Timlin, J. S. Miller, and J. D. Scott, 2004: The atmospheric response to realistic Arctic sea ice anomalies in an AGCM during winter. *J. Climate*, **17**, 890–905, https://doi.org/10.1175/1520-0442(2004)017<0890:TARTRA>2.0.CO;2.

Bader, J., M. D. S. Mesquita, K. I. Hodges, N. Keenlyside, S. Østerhus, and M. Miles, 2011: A review on Northern Hemisphere sea-ice, storminess and the North Atlantic Oscillation: Observations and projected changes. *Atmos. Res.*, **101**, 809–834, https://doi.org/10.1016/j.atmosres.2011.04.007.

Boisvert, L. N., M. A. Webster, A. A. Petty, T. Markus, D. H. Bromwich, and R. I. Cullather, 2018: Intercomparison of precipitation estimates over the Arctic Ocean and its peripheral seas from reanalyses. *J. Climate*, **31**, 8441–8462, https://doi.org/10.1175/JCLI-D-18-0125.1.

Cassano, J. J., P. Uotila, A. H. Lynch, and E. N. Cassano, 2007: Predicted changes in synoptic forcing of net precipitation in large Arctic river basins during the 21st century. *J. Geophys. Res.*, **112**, G04S49, https://doi.org/10.1029/2006JG000332.

Cavalieri, D. J., C. L. Parkinson, P. Gloersen, and H. J. Zwally, 1996, updated yearly. Sea ice concentrations from Nimbus-7 SMMR and DMSP SSM/I-SSMIS passive microwave data, version 1. January 1979–December 2019. NASA National Snow and Ice Data Center Distributed Active Archive Center, accessed 9 February 2021, https://doi.org/10.5067/8GQ8LZQVL0VL.

Comiso, J. C., D. J. Cavalieri, C. L. Parkinson, and P. Gloersen, 1997: Passive microwave algorithms for sea ice concentration: A comparison of two techniques. *Remote Sens. Environ.*, **60**, 357–384, https://doi.org/10.1016/S0034-4257(96)00220-9.

Crasemann, B., D. Handorf, R. Jaiser, K. Dethloff, T. Nakamura, J. Ukita, and K. Yamazaki, 2017: Can preferred atmospheric circulation patterns over the North Atlantic-Eurasian region be associated with Arctic sea ice loss? *Polar Sci.*, **14**, 9–20, https://doi.org/10.1016/j.polar.2017.09.002.

Crawford, A. D., and M. C. Serreze, 2016: Does the summer Arctic Frontal Zone influence Arctic Ocean cyclone activity? *J. Climate*, **29**, 4977–4993, https://doi.org/10.1175/JCLI-D-15-0755.1.

——, and ——, 2017: Projected changes in the Arctic Frontal Zone and summer Arctic cyclone activity in the CESM large ensemble. *J. Climate*, **30**, 9847–9869, https://doi.org/10.1175/JCLI-D-17-0296.1.

——, E. A. P. Schreiber, N. Sommer, M. C. Serreze, J. C. Stroeve, and D. G. Barber, 2021: Sensitivity of Northern Hemisphere cyclone detection and tracking results to fine spatial and temporal resolution using ERA5. *Mon. Wea. Rev.*, **149**, 2581–2598, https://doi.org/10.1175/MWR-D-20-0417.1.

Day, J. J., M. M. Holland, and K. I. Hodges, 2017: Seasonal differences in the response of Arctic cyclones to climate change in CESM1. *Climate Dyn.*, **50**, 3885–3903, https://doi.org/10.1007/s00382-017-3767-x.

Deser, C., J. E. Walsh, and M. S. Timlin, 2000: Arctic sea ice variability in the context of recent atmospheric circulation trends. *J. Climate*, **13**, 617–633, https://doi.org/10.1175/1520-0442(2000)013<0617:ASIVIT>2.0.CO;2.

Eady, E. T., 1949: Long waves and cyclone waves. *Tellus*, **1A**, 33–52, https://doi.org/10.1111/j.2153-3490.1949.tb01265.x.

Finnis, J., M. M. Holland, and M. C. Serreze, 2007: Response of Northern Hemisphere extratropical cyclone activity and associated precipitation to climate change, as represented by the Community Climate System Model. *J. Geophys. Res.*, **112**, G04S42, https://doi.org/10.1029/2006JG000286.

Gelaro, R., and Coauthors, 2017: The Modern-Era Retrospective Analysis for Research and Applications, version 2 (MERRA-2). *J. Climate*, **30**, 5419–5454, https://doi.org/10.1175/JCLI-D-16-0758.1.

Graham, R. M., and Coauthors, 2019a: Winter storms accelerate the demise of sea ice in the Atlantic sector of the Arctic Ocean. *Sci. Rep.*, **9**, 9222, https://doi.org/10.1038/s41598-019-45574-5.

——, and Coauthors, 2019b: Evaluation of six atmospheric reanalyses over Arctic sea ice from winter to early summer. *J. Climate*, **32**, 4121–4143, https://doi.org/10.1175/JCLI-D-18-0643.1.

——, S. R. Hudson, and M. Maturilli, 2019c: Improved performance of ERA5 in Arctic gateway relative to four global atmospheric reanalyses. *Geophys. Res. Lett.*, **46**, 6138–6147, https://doi.org/10.1029/2019GL082781.

Hersbach, H., and Coauthors, 2020: The ERA5 global reanalysis. *Quart. J. Roy. Meteor. Soc.*, **146**, 1999–2049, https://doi.org/10.1002/qj.3803.

Hoskins, B. J., and P. J. Valdes, 1990: On the existence of storm-tracks. *J. Atmos. Sci.*, **47**, 1854–1864, https://doi.org/10.1175/1520-0469(1990)047<1854:OTEOST>2.0.CO;2.

——, and K. I. Hodges, 2019: The annual cycle of Northern Hemisphere storm-tracks. Part 1: Seasons. *J. Climate*, **32**, 1743–1760, https://doi.org/10.1175/JCLI-D-17-0870.1.

IPCC, 2013: *Climate Change 2013: The Physical Science Basis.* Cambridge University Press, 1535 pp., https://doi.org/10.1017/CBO9781107415324.

Jaiser, R., K. Dethloff, D. Handorf, A. Rinke, and J. Cohen, 2012: Impact of sea ice cover changes on the Northern Hemisphere atmospheric winter circulation. *Tellus*, **64A**, 497, https://doi.org/10.3402/tellusa.v64i0.11595.

Kashiwase, H., K. I. Ohshima, S. Nihashi, and H. Eicken, 2017: Evidence for ice-ocean albedo feedback in the Arctic Ocean shifting to a seasonal ice zone. *Sci. Rep.*, **7**, 8170, https://doi.org/10.1038/s41598-017-08467-z.

Koyama, T., J. Stroeve, J. J. Cassano, and A. D. Crawford, 2017: Sea ice loss and Arctic cyclone activity from 1979 to 2014. *J.*

*Climate*, **30**, 4735–4754, https://doi.org/10.1175/JCLI-D-16-0542.1.

Kwok, R., 2018: Arctic sea ice thickness, volume, and multiyear ice coverage: Losses and coupled variability (1958–2018). *Environ. Res. Lett.*, **13**, 105005, https://doi.org/10.1088/1748-9326/aae3ec.

Ledrew, E. F., 1984: The role of local heat sources in synoptic activity within the polar basin. *Atmos.–Ocean*, **22**, 309–327, https://doi.org/10.1080/07055900.1984.9649201.

Li, M., T. Woollings, K. Hodges, and G. Masato, 2014: Extratropical cyclones in a warmer, moister climate: A recent Atlantic analogue. *Geophys. Res. Lett.*, **41**, 8594–8601, https://doi.org/10.1002/2014GL062186.

Lukovich, J. V., J. Stroeve, A. Crawford, L. Hamilton, M. Tsamados, H. Heorton, and F. Massonnet, 2021: Summer extreme cyclone impacts on Arctic sea ice. *J. Climate*, **34**, 4817–4834, https://doi.org/10.1175/JCLI-D-19-0925.1.

Mioduszewski, J., S. Vavrus, and M. Wang, 2018: Diminishing Arctic sea ice promotes stronger surface winds. *J. Climate*, **31**, 8101–8119, https://doi.org/10.1175/JCLI-D-18-0109.1.

Murray, R. J., and I. Simmonds, 1995: Responses of climate and cyclones to reductions in Arctic winter sea ice. *J. Geophys. Res.*, **100**, 4791–4806, https://doi.org/10.1029/94JC02206.

Neu, U., and Coauthors, 2013: IMILAST: A community effort to intercompare extratropical cyclone detection and tracking algorithms. *Bull. Amer. Meteor. Soc.*, **94**, 529–547, https://doi.org/10.1175/BAMS-D-11-00154.1.

Onarheim, I. H., T. Eldevik, L. H. Smedsrud, and J. C. Stroeve, 2018: Seasonal and regional manifestation of Arctic sea ice loss. *J. Climate*, **31**, 4917–4932, https://doi.org/10.1175/JCLI-D-17-0427.1.

Pierrehumbert, R. T., and K. L. Swanson, 1995: Baroclinic instability. *Annu. Rev. Fluid Mech.*, **27**, 419–467, https://doi.org/10.1146/annurev.fl.27.010195.002223.

Raddatz, R. L., R. J. Galley, and D. G. Barber, 2012: Linking the atmospheric boundary layer to the Amundsen Gulf sea-ice cover: A mesoscale to synoptic-scale perspective from winter to summer 2008. *Bound.-Layer Meteor.*, **142**, 123–148, https://doi.org/10.1007/s10546-011-9669-2.

Renfrew, I. A., and Coauthors, 2021: An evaluation of surface meteorology and fluxes over the Iceland and Greenland Seas in ERA5 reanalysis: The impact of sea ice distribution. *Quart. J. Roy. Meteor. Soc.*, **147**, 691–712, https://doi.org/10.1002/qj.3941.

Rinke, A., W. Maslowski, K. Dethloff, and J. Clement, 2006: Influence of sea ice on the atmosphere: A study with an Arctic atmospheric regional climate model. *J. Geophys. Res. Atmos.*, **111**, D16103, https://doi.org/10.1029/2005JD006957.

Rohrer, M., O. Martius, C. C. Raible, and S. Brönnimann, 2020: Sensitivity of blocks and cyclones in ERA5 to spatial resolution and definition. *Geophys. Res. Lett.*, **47**, 223, https://doi.org/10.1029/2019GL085582.

Royer, J. F., S. Planton, and M. Déqué, 1990: A sensitivity experiment for the removal of Arctic sea ice with the French spectral general circulation model. *Climate Dyn.*, **5** (1), 1–17, https://doi.org/10.1007/BF00195850.

Schreiber, E. A. P., and M. C. Serreze, 2020: Impacts of synoptic-scale cyclones on Arctic sea-ice concentration: A systematic analysis. *Ann. Glaciol.*, **61**, 139–153, https://doi.org/10.1017/aog.2020.23.

Schweiger, A. J., R. W. Lindsay, S. Vavrus, and J. A. Francis, 2008: Relationships between Arctic sea ice and clouds during autumn. *J. Climate*, **21**, 4799–4810, https://doi.org/10.1175/2008JCLI2156.1.

Screen, J. A., and I. Simmonds, 2010: The central role of diminishing sea ice in recent Arctic temperature amplification. *Nature*, **464**, 1334–1337, https://doi.org/10.1038/nature09051.

——, ——, and K. Keay, 2011: Dramatic interannual changes of perennial Arctic sea ice linked to abnormal summer storm activity. *J. Geophys. Res.*, **116**, D15105, https://doi.org/10.1029/2011JD015847.

——, ——, C. Deser, and R. Tomas, 2013: The atmospheric response to three decades of observed Arctic sea ice loss. *J. Climate*, **26**, 1230–1248, https://doi.org/10.1175/JCLI-D-12-00063.1.

Seierstad, I. A., and J. Bader, 2008: Impact of a projected future Arctic sea ice reduction on extratropical storminess and the NAO. *Climate Dyn.*, **33**, 937–943, https://doi.org/10.1007/s00382-008-0463-x.

Seo, H., and J. Yang, 2013: Dynamical response of the Arctic atmospheric boundary layer process to uncertainties in sea-ice concentration. *J. Geophys. Res. Atmos.*, **118**, 12 383–12 402, https://doi.org/10.1002/2013JD020312.

Serreze, M. C., and W. N. Meier, 2019: The Arctic's sea ice cover: Trends, variability, predictability, and comparisons to the Antarctic. *Ann. N. Y. Acad. Sci.*, **1436**, 36–53, https://doi.org/10.1111/nyas.13856.

——, F. Carse, R. G. Barry, and J. C. Rogers, 1997: Icelandic low cyclone activity: Climatological features, linkages with the NAO, and relationships with recent changes in the Northern Hemisphere circulation. *J. Climate*, **10**, 453–464, https://doi.org/10.1175/1520-0442(1997)010<0453:ILCACF>2.0.CO;2.

——, A. P. Barrett, J. C. Stroeve, D. N. Kindig, and M. M. Holland, 2009: The emergence of surface-based Arctic amplification. *Cryosphere*, **3**, 11–19, https://doi.org/10.5194/tc-3-11-2009.

Simmonds, I., and K. Keay, 2009: Extraordinary September Arctic sea ice reductions and their relationships with storm behavior over 1979–2008. *Geophys. Res. Lett.*, **36**, L19715, https://doi.org/10.1029/2009GL039810.

——, and I. Rudeva, 2012: The great Arctic cyclone of August 2012. *Geophys. Res. Lett.*, **39**, L23709, https://doi.org/10.1029/2012GL054259.

——, and ——, 2014: A comparison of tracking methods for extreme cyclones in the Arctic basin. *Tellus*, **66A**, 25252, https://doi.org/10.3402/tellusa.v66.25252.

——, and M. Li, 2021: Trends and variability in polar sea ice, global atmospheric circulations, and baroclinicity. *Ann. N. Y. Acad. Sci.*, **1504**, 167–186, https://doi.org/10.1111/nyas.14673.

Smith, D. M., and Coauthors, 2019: The Polar Amplification Model Intercomparison Project (PAMIP) contribution to CMIP6: Investigating the causes and consequences of polar amplification. *Geosci. Model Dev.*, **12**, 1139–1164, https://doi.org/10.5194/gmd-12-1139-2019.

Song, J.-N., G. Fu, Y. Xu, Z.-Y. Han, Q.-Z. Sun, and H. Wang, 2021: Assessment of the capability of CMIP6 global climate models to simulate Arctic cyclones. *Adv. Climate Change Res.*, 12, 660–676, https://doi.org/10.1016/j.accre.2021.07.007.

Stewart, R. E., and N. R. Donaldson, 1989: On the nature of rapidly deepening Canadian East Coast winter storms. *Atmos.–Ocean*, **27**, 87–107, https://doi.org/10.1080/07055900.1989.9649329.

Stroeve, J., and D. Notz, 2018: Changing state of Arctic sea ice across all seasons. *Environ. Res. Lett.*, **13**, 103001, https://doi.org/10.1088/1748-9326/aade56.

——, M. C. Serreze, A. Barrett, and D. N. Kindig, 2011: Attribution of recent changes in autumn cyclone associated

precipitation in the Arctic. *Tellus*, **63A**, 653–663, https://doi.org/10.1111/j.1600-0870.2011.00515.x.

——, ——, M. M. Holland, J. E. Kay, J. A. Maslanik, and A. P. Barrett, 2012: The Arctic's rapidly shrinking sea ice cover: A research synthesis. *Climatic Change*, **110**, 1005–1027, https://doi.org/10.1007/s10584-011-0101-1.

Tanaka, H. L., A. Yamagami, and S. Takahashi, 2012: The structure and behavior of the Arctic cyclone in summer analyzed by the JRA-25/JCDAS data. *Polar Sci.*, **6**, 55–69, https://doi.org/10.1016/j.polar.2012.03.001.

Thorncroft, C. D., B. J. Hoskins, and M. E. McIntyre, 1993: Two paradigms of baroclinic-wave life-cycle behaviour. *Quart. J. Roy. Meteor. Soc.*, **119**, 17–55, https://doi.org/10.1002/qj.49711950903.

Ulbrich, U., G. C. Leckebusch, and J. G. Pinto, 2009: Extra-tropical cyclones in the present and future climate: A review. *Theor. Appl. Climatol.*, **96**, 117–131, https://doi.org/10.1007/s00704-008-0083-8.

Valkonen, E., J. Cassano, and E. Cassano, 2021: Arctic cyclones and their interactions with declining sea ice: A recent climatology. *J. Geophys. Res. Atmos.*, **126**, e2020JD034366, https://doi.org/10.1029/2020JD034366.

Vessey, A. F., K. I. Hodges, L. C. Shaffrey, and J. J. Day, 2020: An inter-comparison of Arctic synoptic scale storms between four global reanalysis datasets. *Climate Dyn.*, **54**, 2777–2795, https://doi.org/10.1007/s00382-020-05142-4.

Villamil-Otero, G. A., J. Zhang, J. He, and X. Zhang, 2017: Role of extratropical cyclones in the recently observed increase in poleward moisture transport into the Arctic Ocean. *Adv. Atmos. Sci.*, **35**, 85–94, https://doi.org/10.1007/s00376-017-7116-0.

Wallace, J. M., and P. V. Hobbs, 2006: *Atmospheric Science: An Introductory Survey*. 2nd ed. R. Dmowska, D. Hartmann, and H. T. Rossby, Eds. Academic Press, 483 pp.

Walter, B. A., J. E. Overland, and P. Turet, 1995: A comparison of satellite-derived and aircraft-measured regional surface sensible heat fluxes over the Beaufort Sea. *J. Geophys. Res. Oceans*, **100**, 4585–4591, https://doi.org/10.1029/94JC02653.

Webster, M. A., C. Parker, L. Boisvert, and R. Kwok, 2019: The role of cyclone activity in snow accumulation on Arctic sea ice. *Nat. Commun.*, **10**, 5285, https://doi.org/10.1038/s41467-019-13299-8.

Wei, L., T. Qin, and C. Li, 2017: Seasonal and inter-annual variations of Arctic cyclones and their linkage with Arctic sea ice and atmospheric teleconnections. *Acta Oceanol. Sin.*, **36** (10), 1–7, https://doi.org/10.1007/s13131-017-1117-9.

Wernli, H., and L. Papritz, 2018: Role of polar anticyclones and mid-latitude cyclones for Arctic summertime sea-ice melting. *Nat. Geosci.*, **11**, 108–113, https://doi.org/10.1038/s41561-017-0041-0.

Yang, J., J. Comiso, D. Walsh, R. Krishfield, and S. Honjo, 2004: Storm-driven mixing and potential impact on the Arctic Ocean. *J. Geophys. Res.*, **109**, C04008, https://doi.org/10.1029/2001JC001248.

Yettella, V., and J. E. Kay, 2017: How will precipitation change in extratropical cyclones as the planet warms? Insights from a large initial condition climate model ensemble. *Climate Dyn.*, **49**, 1765–1781, https://doi.org/10.1007/s00382-016-3410-2.

Zhang, J., R. Lindsay, A. Schweiger, and M. Steele, 2013: The impact of an intense summer cyclone on 2012 Arctic sea ice retreat. *Geophys. Res. Lett.*, **40**, 720–726, https://doi.org/10.1002/grl.50190.